

Production of ϕ Mesons in Au + Au Collisions at $11.7A\text{GeV}/c$

B.B. Back,¹ R.R. Betts,^{1,2} J. Chang,³ W.C. Chang,^{3,*} C.Y. Chi,⁴ Y.Y. Chu,⁵ J.B. Cumming,⁵ J.C. Dunlop,^{6,†} W. Eldredge,³ S.Y. Fung,³ R. Ganz,² E. Garcia,⁷ A. Gillitzer,^{1,‡} G. Heintzelman,^{6,†} W.F. Henning,^{1,§} D.J. Hofman,^{1,¶} B. Holzman,^{2,†} J.H. Kang,⁸ E.J. Kim,⁸ S.Y. Kim,⁸ Y. Kwon,⁸ D. McLeod,² A.C. Mignerey,⁷ M. Moulson,^{4,**} V. Nanal,^{1,††} C.A. Ogilvie,^{6,††} R. Pak,^{9,†} A. Ruangma,⁷ D.E. Russ,^{7,§§} R.K. Seto,³ P.J. Stanskas,⁷ G.S.F. Stephans,⁶ H.Q. Wang,^{3,¶¶} F.L.H. Wolfs,⁹ A.H. Wuosmaa,¹ H. Xiang,³ G.H. Xu,³ H.B. Yao,⁶ and C.M. Zou^{3,***}

(E917 Collaboration)

¹Argonne National Laboratory, Argonne, IL 60439, USA

²University of Illinois at Chicago, Chicago, IL 60607, USA

³University of California, Riverside, CA 92521, USA

⁴Columbia University, Nevis Laboratories, Irvington, NY 10533, USA

⁵Brookhaven National Laboratory, Upton, NY 11973, USA

⁶Massachusetts Institute of Technology, Cambridge, MA 02139, USA

⁷University of Maryland, College Park, MD 20742, USA

⁸Yonsei University, Seoul 120-749, South Korea

⁹University of Rochester, Rochester, NY 14627, USA

We report on a measurement of ϕ -meson production in Au + Au collisions at a beam momentum of $11.7A\text{GeV}/c$ by Experiment E917 at the AGS. The measurement covers the midrapidity region $1.2 < y < 1.6$. Transverse-mass spectra and rapidity distribution are presented as functions of centrality characterized by the number of participant projectile nucleons. The yield of ϕ 's per participant projectile nucleon increases strongly in central collisions in a manner similar to that observed for kaons.

PACS numbers: 25.75.-q, 25.75.Dw, 13.85.Ni

I. INTRODUCTION

The production of ϕ mesons in relativistic heavy-ion collisions has been an important subject of study at the AGS, the SPS, and the newly operating RHIC facility. The production of the ϕ meson, the lightest bound state of strange quarks ($s\bar{s}$), is suppressed in ordinary hadronic interactions because of the Okubo-Zweig-Iizuka (OZI) rule [1]. It has been proposed that in a quark-gluon plasma (QGP) scenario, strange quarks

could be rapidly and abundantly produced via gluon interactions [2]. Thus, ϕ mesons could be created in a non-conventional way via strange quark coalescence, bypassing the OZI rule. A strong enhancement in ϕ -meson production would serve as one of the strangeness-enhancement signatures for QGP formation [3].

The production of ϕ mesons has been measured in Si + Au collisions at $14.6A\text{GeV}/c$ by E859 at the AGS within a rapidity coverage of $1.2 < y < 2.0$ [4]. It was found that the ratio of the total ϕ yield relative to the K^- yield was 10% for the uppermost 7% of the charged particle multiplicity distribution. NA49 at the SPS has measured ϕ -meson production in $p+p$, $p+\text{Pb}$, and $\text{Pb}+\text{Pb}$ collisions at a beam energy (E_{beam}) of 158 AGeV within a rapidity range of $3.0 < y < 3.8$. An enhancement in the ratio of ϕ to pion total yields by a factor of 3.0 ± 0.7 was observed in central $\text{Pb} + \text{Pb}$ collisions relative to $p + p$ interactions [5]. Also at the SPS, NA38/NA50 have measured the ratio $\phi/(\rho+\omega)$ by fitting the invariant-mass spectrum of muon pairs and found a steady increase of this ratio with centrality, up to unity in the most central bin, in $\text{Pb} + \text{Pb}$ collisions within $0 < y < 1$ and $1.5 < m_t < 3.2 \text{ GeV}/c^2$ [6]. Recently, the STAR experiment reported on a measurement of the ϕ yield at midrapidity in Au + Au collisions at center-of-mass energy $\sqrt{s_{NN}} = 130 \text{ GeV}$. An increase in the ϕ/h^- ratio with $\sqrt{s_{NN}}$ was observed [7].

Enhancements in the yields of particles with open strangeness have also been observed, both at the AGS and the SPS. At the AGS, K^+/π^+ ratios were seen to increase to $\sim 20\%$ in central Si + Au and Au + Au collisions,

*Present address: Institute of Physics, Academia Sinica, Taipei 11529, Taiwan.

†Present address: Brookhaven National Laboratory, Upton, NY 11973, USA.

‡Present address: Forschungszentrum Jülich, Jülich, D-52425, Germany.

§Present address: Gesellschaft für Schwerionenforschung, D-64291 Darmstadt, Germany.

¶Present address: University of Illinois at Chicago, Chicago, IL 60607.

**Present address: Laboratori Nazionali di Frascati dell'INFN, 00044 Frascati RM, Italy.

††Present address: Tata Institute of Fundamental Research, Colaba, Mumbai 400005, India.

††Present address: Iowa State University, Ames, IA 50011.

§§Present address: National Institute of Health, Gaithersburg, MD 20892.

¶¶Present address: CW Associates, 7676 Woodbine, Markham L3R 2N2, Ontario.

***Present address: H.-M. Zou, Rabobank Nederland, 245 Park Ave, New York, NY 10167.

from 4–8% in $p + p$ collisions [8, 9, 10], and the $\bar{\Lambda}/\bar{p}$ ratio was found to increase strongly with centrality in Au + Au collisions [11, 12]. At the SPS, the WA97 collaboration has observed enhanced production of K 's, Λ 's, Ξ 's, and Ω 's in heavy-ion collisions relative to $p + p$ or $p + A$ collisions [13]. Measurements from the PHENIX experiment at center-of-mass energy $\sqrt{s_{NN}} = 130$ GeV showed the kaon yield to be more strongly dependent on centrality than the pion yield at midrapidity [14].

The reason for the strangeness enhancement in heavy-ion collisions is not completely understood. The rescattering of hadrons and the conversion of the excitation energy of secondary resonances into strange particles might give rise to strangeness enhancement in a purely hadronic picture [15, 16, 17]. Strangeness enhancement could also be interpreted as a reduction in canonical strangeness suppression from $p + p$ to $A + A$ reactions in the context of thermal models [18]. Strangeness enhancement as a function of the number of “grey” protons (a centrality index) has also been seen in $p + A$ collisions, in which a QGP phase is unlikely to contribute [19].

Under the conventional hadronic interactions, there are mainly three scenarios proposed for the production of ϕ mesons in nuclear collisions:

- Parton fusion of strange sea quarks [20] or knock-out of $s\bar{s}$ pairs [21] from the primary collisions of projectile and target nucleons.
- Secondary baryon-baryon interactions $BB \rightarrow \phi NN$, meson-baryon interactions $(\pi, \rho)B \rightarrow \phi B$ [22] and meson-meson interactions $\pi\rho \rightarrow \phi$ [23], where $B = N, \Delta, N^*$.
- Secondary kaon-hyperon interactions $K\Lambda \rightarrow \phi N$ and kaon-antikaon scattering $KK \rightarrow \phi\rho$ in the event of the restoration of chiral symmetry in hot and dense nuclear fireball [24].

With inclusion of secondary meson-baryon and meson-meson interactions, RQMD (Relativistic Quantum Molecular Dynamics) [23] is able to qualitatively describe the increase of kaon yields with centrality measured by E866 [25], though quantitative differences do exist [26].

As can be seen, the production of ϕ 's couples with that of other hadrons, such as kaons and pions. Hence, a systematic measurement of ϕ production in different collisional systems may help to quantify the increase in the overall strangeness production, and, in combination with other measurements of strange and non-strange hadron production, to differentiate between possible mechanisms contributing to the strangeness enhancement [27].

In this paper we report on a measurement of the ϕ yield around midrapidity in Au + Au collisions at the Alternating Gradient Synchrotron (AGS) at Brookhaven National Laboratory (BNL), and compare it to the yields of pions and kaons.

II. EXPERIMENTAL DETAILS

Experiment E917 took data on Au + Au reactions at projectile momenta of 6.8, 8.9 and 11.7 A GeV/c (corresponding to center-of-mass energy $\sqrt{s_{NN}} = 3.83, 4.31$, and 4.87 GeV, respectively) in the fall of 1996. The identified particles include particles containing strange quarks, such as K^+ , K^- , ϕ , Λ , and $\bar{\Lambda}$, and non-strange particles such as π , p , and \bar{p} [10, 12, 28, 29, 30]. The experimental apparatus consisted of a movable magnetic spectrometer for tracking and particle identification, and beamline detector arrays for global event characterization. When the data reported in this work were collected, the beam momentum was 11.7 A GeV/c and the spectrometer angle was set to either 14° or 19° from the beam axis. The momentum resolution of the spectrometer, $\delta p/p$, was about 1% for particles with momentum greater than 1 GeV/c and increased at lower momentum, up to 2% at $p = 0.6$ GeV/c, due to the effect of multiple-scattering. The kaon momenta in reconstructed ϕ events mostly lay in the range of $1.0 < p < 2.0$ GeV/c. Event centrality was characterized by the energy of the beam spectators after the interaction as measured in the zero-degree calorimeter (ZCAL), positioned downstream of the target on the beam axis. More details on the detector systems are given in Refs. [30, 31, 32].

The data presented here were collected using a two-level online trigger: a minimum-bias interaction trigger (LVL1) followed by a particle-identification trigger (LVL2) which required two charged kaons of either sign or one \bar{p} in the spectrometer acceptance. The hardware LVL2 trigger looped over the combinations of drift chamber and TOF hits, and formed combinations consistent with tracks corresponding to particles of various momenta, charge, and particle type using a look-up table [33]. The LVL2 trigger increased the live time of data acquisition system by essentially the ratio of the rate of vetoable LVL1 triggers to the rate of vetoable LVL1 triggers that were not vetoed. This ratio was known as the LVL2 rejection factor, and could be estimated online. In Au+Au collisions with a field of 4KG and the spectrometers at 14° and 19° , typical rejection factors for a $K^+/K^-/\bar{p}$ trigger were 4.8 and 8.5, respectively. By examining data that was taken with LVL1 trigger and recording the decision of LVL2, the inefficiency of LVL2 trigger was monitored and found to be less than 1% for events fully inside the acceptance. Most of the LVL2 triggered data was background since the trigger was optimized to reject only events that were clearly not of the correct type to keep the efficiency near 100%.

A time-of-flight (TOF) system with a typical resolution of 130 ps served to identify pions and kaons up to a momentum of 1.75 GeV/c with 3 standard deviations of TOF resolution. Above this momentum, the 3σ contours in the (p, TOF) plane began to overlap. Within this region, particles were identified as kaons only if their TOF was inside the kaon region and outside of the pion region, since 10–30% of the tracks in the overlap region were from

TABLE I: Centrality bins used in the analysis. The cuts on zero-degree energy, E_{ZCAL} , that define each bin are listed (in GeV), together with the corresponding fraction of the geometrical cross section for Au + Au collisions (in percent), the mean number of projectile participants for the bin, $\langle N_{\text{pp}} \rangle$, and the estimated value of the mean number of binary collisions, $\langle N_{\text{coll}} \rangle$, by Glauber model and the mean number of projectile participants estimated from E_{ZCAL} , $\langle N_{\text{pp}}^{\text{ZCAL}} \rangle$. The total beam kinetic energy in the collisions is about 2123 GeV.

bin	E_{ZCAL}	% σ_{geom}	$\langle N_{\text{pp}} \rangle$	$\langle N_{\text{coll}} \rangle$	$\langle N_{\text{pp}}^{\text{ZCAL}} \rangle$
1	0-280	0-5	170 ± 10	770 ± 72	179 ± 1.0
2	280-560	5-12	138 ± 12	585 ± 74	157 ± 1.5
3	560-960	12-23	101 ± 14	393 ± 74	126 ± 2.0
4	960-1440	23-39	62 ± 14	207 ± 60	84 ± 2.6
5	>1440	39-77	20 ± 12	50 ± 38	34 ± 3.1

pions. The kaon identification inefficiency from the exclusion of pion bands in this region of high momenta was corrected by extra weighting. Additionally, kaons with momenta less than $0.5 \text{ GeV}/c$ were rejected to avoid the need for large acceptance corrections.

The data were weighted to correct for experimental inefficiency from the following effects: spectrometer acceptance, kaon decays in flight, single-particle tracking inefficiency, hadronic interaction, multiple scattering in the spectrometer, momentum cuts, the two-track opening angle cut, the kaon identification inefficiency, and the branching ratio for the decay $\phi \rightarrow K^+ K^-$. The effects were studied individually using a GEANT-based Monte Carlo simulation implementing a realistic detector configuration [32]. Weights were applied on a track-by-track basis except for those for the two-track opening angle cut and branching ratio correction. The spectrometer acceptance was evaluated for each pair in bins of rapidity and transverse mass. An additional correction for the single-track tracking efficiency in the presence of background hits on the drift chambers was evaluated by inserting found tracks into random events. This occupancy correction was then parameterized by the hit multiplicity in the chambers and applied for each track. The resulting occupancy correction was typically 20–40%.

The index of event centrality was obtained from the measurement of the energy deposited in the zero-degree calorimeter, E_{ZCAL} . Assuming a monotonic relation between the energy deposition in the calorimeter and the event centrality such that the most central events correspond to the smallest energy deposition, we have divided the data into five centrality bins. We have attempted to estimate $\langle N_{\text{pp}} \rangle$, the mean number of projectile participants, and $\langle N_{\text{coll}} \rangle$, the mean number of binary collisions, according to the Glauber model [34], using impact parameter cuts corresponding to the centrality range for each bin (expressed as a fraction of the 6.8 b geometrical cross section for Au + Au collisions, as listed in the Table I), and an assumed $p + p$ inelastic cross section

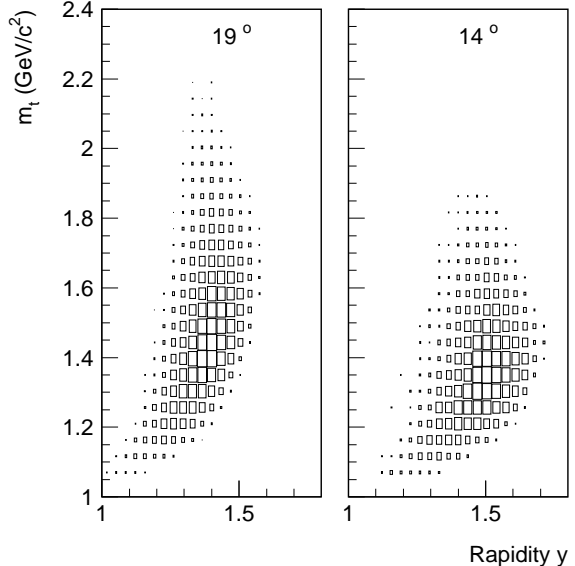


FIG. 1: The experimental acceptance for $K^+ K^-$ pairs in the space of transverse mass (m_t) vs. rapidity (y) for the two spectrometer angle settings at 19° and 14° .

of 30 mb. In Exps. 802, 856 and 866 [9], the number of projectile participants has been conventionally estimated from the relation $N_{\text{pp}}^{\text{ZCAL}} = A_{\text{proj}}(1 - E_{\text{ZCAL}}/E_{\text{beam}})$, where A_{proj} is the atomic mass of the projectile, and E_{beam} is the total kinetic energy of the nuclei in the beam before interaction, which was 2123 GeV in the present case. For the purpose of comparison, we also calculated $N_{\text{pp}}^{\text{ZCAL}}$ and its uncertainty with a nominal ZCAL energy resolution (σ_E/E) of 3.6% [35]. All relevant parameters for each centrality bin are listed in Table I. To facilitate a comparison with other experiments we will use $\langle N_{\text{pp}} \rangle$ calculated using the Glauber model for the rest of this paper.

III. EXPERIMENTAL RESULTS

A total of 250 million LVL2-triggered events were analyzed. When the two spectrometer angle settings were combined, the overall acceptance for $K^+ K^-$ pairs covered the region of rapidity $1.2 < y < 1.6$ and transverse mass $1.0 \text{ GeV}/c^2 < m_t (\equiv \sqrt{m_\phi^2 + (p_t/c)^2}) < 2.2 \text{ GeV}/c^2$, as shown in Fig. 1. Experimental results from both the 14° and 19° settings of the spectrometer were consistent within statistical errors and combined for the presentation of the transverse-mass spectra.

The ϕ mesons were reconstructed from the invariant-mass (m_{inv}) distribution of identified $K^+ K^-$ pairs and subtracting the combinatorial background which was obtained by the event-mixing method [36]. Two kinds of

distributions were formed: “same-event” distributions, in which the K^+ ’s and K^- ’s were selected from the same event, and “mixed-event” distributions, in which the individual particles were chosen from different events in the same centrality class to represent the uncorrelated background.

A. Invariant-mass distribution for K^+K^- pairs

First, we examined the minimum bias invariant mass distribution of kaon pairs by fitting the data to a relativistic Breit-Wigner distribution (RBW) convoluted with a Gaussian representing the experimental mass resolution [4, 37]. The shape of the background (BG) was obtained from the mixed event distribution while the normalization was left as a free parameter in the fit. The parameterization is as follows:

$$\frac{dN_{K^+K^-}^{same}}{dm} = a \int_{m_1}^{m_2} \text{RBW}(m') \frac{\exp\left[-\frac{1}{2}(\frac{m-m'}{\sigma_m})^2\right]}{\sqrt{2\pi\sigma_m^2}} dm' + b \frac{dN_{K^+K^-}^{mixed}}{dm}, \quad (1)$$

where

$$\text{RBW}(m) = \frac{mm_0\Gamma(m)}{(m^2 - m_0^2)^2 + (m_0\Gamma(m))^2}, \quad (2)$$

$$\Gamma(m) = 2\Gamma_0 \frac{(q/q_0)^3}{(q/q_0)^2 + 1}, \quad (3)$$

$$q_0 = \sqrt{m_0^2/4 - m_K^2}, \quad (4)$$

$$q = \sqrt{m^2/4 - m_K^2}, \quad (5)$$

and where the limits of integration were $m_1 = 0.989 \text{ GeV}/c^2$ and $m_2 = 1.252 \text{ GeV}/c^2$. There were five free parameters in all: the relative normalizations a and b , the peak mass and width parameters m_0 and Γ_0 , and the experimental mass resolution σ_m .

For the minimum-bias data, the same-event invariant-mass distribution of K^+K^- pairs and the background-subtracted signal distribution corresponding to the first term in Eq. (1), are shown together with the fits in Fig. 2. The values $m_0 = 1018.99 \pm 0.36 \text{ MeV}/c^2$, $\Gamma_0 = 6.14 \pm 2.59 \text{ MeV}/c^2$ and $\sigma_m = 2.43 \pm 1.11 \text{ MeV}/c^2$ were obtained with $\chi^2/\text{dof} = 0.87$. The fitted peak position (m_0) and width (Γ_0) of the ϕ signal were in agreement with the world-average values. The large uncertainty on Γ_0 arose mostly because of a high degree of correlation in the fit between the values for the parameters Γ_0 and b (correlation coefficient = 0.71). The experimental mass resolution (σ_m) was also consistent with our estimated value of $2.0 \text{ MeV}/c^2$, from Monte Carlo studies and from the width of the peak from Λ decay in the $p\pi^-$ invariant-mass distribution [32] (the known contribution from the multiple scattering of the kaons in the target in

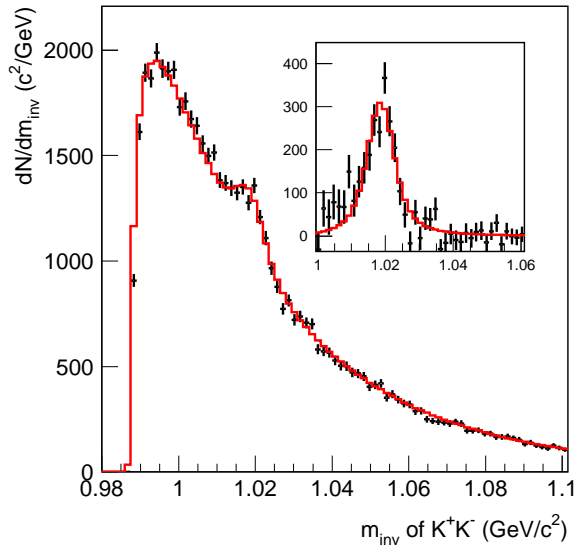


FIG. 2: (Color Online) The invariant mass (m_{inv}) distribution of K^+K^- pairs for minimum-bias events, superimposed with a fitted distribution of a relativistic Breit-Wigner distribution plus the background distribution from a mixed-event technique, as described in the text. In the inset, the ϕ signal together with fitted results of the first term in Eq. (1) is shown.

the case of the present measurement was accounted for by additional smearing). It is noted that the result of the fit lay systematically below the data in the invariant-mass region $10-20 \text{ MeV}/c^2$ below the ϕ peak. We did not have a clear understanding of this effect.

B. Transverse-mass spectra and rapidity distributions

Monte Carlo studies confirmed that the experimental invariant-mass resolution (σ_m) remained constant ($\sim 2 \text{ MeV}/c^2$) across the kinematic region of acceptance [32]. Given the stable mass resolution and the limited statistics for the division of data into bins in centrality and phase space, the transverse-mass spectra were obtained by counting events in a defined signal window and estimating the number of background events within this window, rather than by the integration of the result of the fit with Eq. (1). The details were as follows. Data were divided into subsets for each of the two spectrometer settings and five centrality classes. Same-event and mixed-event pairs for each subset were binned in rapidity and transverse mass ($\Delta y = 0.2$ and $\Delta m_t = 0.2 \text{ GeV}/c^2$), and invariant-mass distributions were obtained for each bin. In each bin, the total number of signal and background counts ($S + B$) was taken to be the sum of the counts within a signal window defined as $0.9995 <$

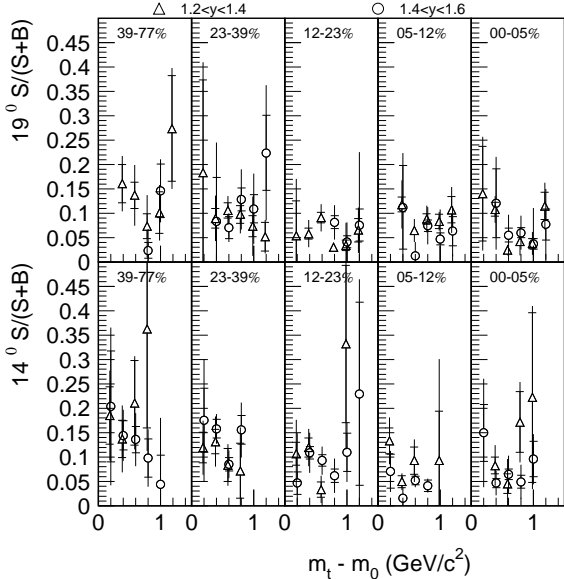


FIG. 3: The signal-to-total ratio ($S/(S+B)$) of ϕ 's as a function of transverse mass ($m_t - m_0$) in five centrality bins, labeled by $\sigma/\sigma_{\text{geom}}$. The top panel is for the data with the spectrometer at 19° while the bottom one for 14° . Solid (open) symbols represent points from $1.2 < y < 1.4$ ($1.4 < y < 1.6$). The total errors are calculated as the quadrature sum of the systematic and statistical errors, while the magnitude of the latter is indicated by the cross bars.

$m_{\text{inv}} < 1.0385$ GeV/ c^2 . We then estimated the number of background counts (B) inside the signal window as the number of counts in the normalized distribution of mixed-event pairs in this same interval. The normalization factor was determined by a log-likelihood fit of the mixed-event distribution to the same-event distribution in the region outsides the signal window. The final number of signal counts was obtained by subtracting the background estimated in this way from the total number of events in the signal window.

In Fig. 3, the signal-to-total ratio ($S/(S+B)$) for two spectrometer-angle settings and five centrality bins are plotted as a function of the transverse mass ($m_t - m_0$) of K^+K^- pairs. These ratios decreased with centrality as expected. The statistical error on S was calculated as $\sqrt{(S+B) + B}$ and the error on B is estimated from the fitting error of the normalization factor for the mixed-event distribution. The final cross section was then calculated by applying the weights from the acceptance and other experimental effects as mentioned above.

The transverse-mass spectra for the five centrality bins are shown in two bins of rapidity, $1.2 < y < 1.4$ and $1.4 < y < 1.6$, with an m_t bin size of 0.2 GeV/ c^2 in Fig. 4. For the m_t bins where the acceptance from 14° and 19° data sets overlap, the weighted average of the two measurements is presented after checking for consistency. The full error shown includes both statistical and

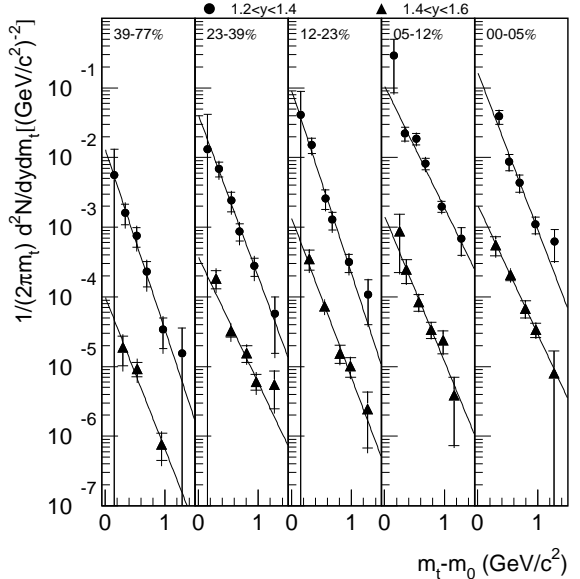


FIG. 4: The invariant yield of ϕ 's as a function of transverse mass ($m_t - m_0$) in five centrality bins labeled by $\sigma/\sigma_{\text{geom}}$. In each panel, the top set of points of circles is for $1.2 < y < 1.4$, while the second set of points of triangles is for $1.4 < y < 1.6$ and is divided by 100 for presentation. The total errors are calculated as the quadrature sum of the systematic and statistical errors, while the magnitude of the latter is indicated by the cross bars. The lines are the results of the exponential fits described in the text.

systematic contributions; the contribution from statistics alone is indicated by the cross bars. The total errors are calculated as the quadrature sum of the statistical and systematic errors. Systematic errors are estimated to range from about 15% in the most central bin to 30% for the most peripheral bin.

There were two main sources of systematic errors: the uncertainties in the ZCAL centrality cut and the determination of $S/(S+B)$. Due to the radiation damage of the plastic scintillator materials of the ZCAL, its signal decreased with time and a run-dependent calibration was necessary. The calibrations were performed in a few separate periods of run time and we estimated the systematic uncertainty of the run-independent ZCAL cuts for the definition of these five centrality bins. The effect on the cross section of varying the ZCAL cuts within their uncertainties was included in the systematic error on each cross-section point. A systematic error for $S/(S+B)$ was estimated by varying the width of the defined signal window from $\pm 2\Gamma_0$ to $\pm 5\Gamma_0$ and thus the corresponding regions for normalization fitting.

An exponential parameterization with two parameters, rapidity density (dN/dy), and inverse slope (T), was used to fit the transverse-mass spectra:

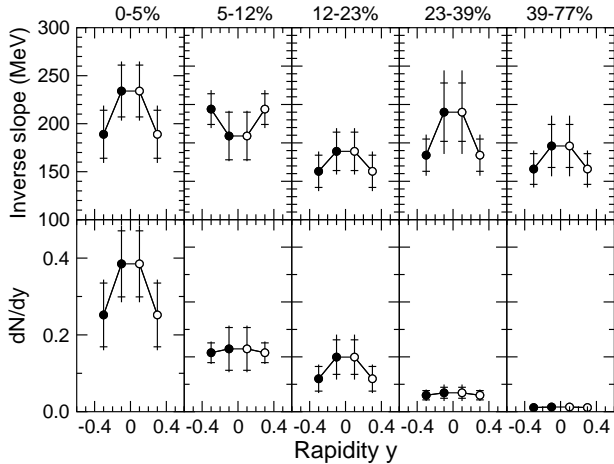


FIG. 5: The inverse slope parameters, T , and rapidity density, dN/dy , of ϕ mesons as a function of centrality. The open symbols show the reflections of the data points about midrapidity ($y = 1.6$). The error bars have the same significance as in Fig. 4.

$$\frac{1}{2\pi c^4 m_t} \frac{d^2 N}{dm_t dy} = \frac{dN/dy}{2\pi(T m_0 c^2 + T^2)} \times \exp\left(-\frac{(m_t - m_0)c^2}{T}\right). \quad (6)$$

This function gave a good fit to the data with $\chi^2/\text{dof} \sim 1$ in all cases. The values obtained for rapidity density (dN/dy) and inverse slope parameters (T) are plotted as functions of rapidity and centrality in Fig. 5 and are listed in Tabs. II and III. As a function of centrality, the rapidity density shows a strong systematic increase, while the inverse slope increases more mildly. Within the rapidity range covered by the measurement, there seems to be no strong rapidity dependence for T .

The fiducial yield is the sum of the values $dN/dy \times \Delta y$ for the two rapidity bins covering the interval $1.2 < y < 1.6$ and is plotted as a function of $\langle N_{\text{pp}} \rangle$ (calculated from a Glauber model as explained in Sec. II) in Fig. 6. When normalized to $\langle N_{\text{pp}} \rangle$, this quantity exhibits a steady increase with increasing centrality as shown in Fig. 6. This implies that the fiducial yield of ϕ 's increases faster than a linear scaling with $\langle N_{\text{pp}} \rangle$. It is noted that a little more drastic increase in centrality (in the order of 4% effect in the slope with a linear fit) is observed if the fiducial yields are plotted against $\langle N_{\text{pp}}^{\text{ZCAL}} \rangle$. Thus, we observe an enhancement in ϕ -meson production in central events. This is similar to what has been previously observed for kaon production [9].

IV. DISCUSSION

In this section, we compare the measured inverse slopes (T) and rapidity densities (dN/dy) for the ϕ to those

TABLE II: Inverse slope parameter, T , in units of MeV, for ϕ 's in two bins of rapidity and five bins of centrality. Errors are statistical followed by systematic.

Centrality	$1.2 < y < 1.4$	$1.4 < y < 1.6$
0-5%	$189 \pm 25 \pm 16$	$234 \pm 27 \pm 15$
5-12%	$244 \pm 20 \pm 14$	$209 \pm 31 \pm 9$
12-23%	$163 \pm 21 \pm 15$	$189 \pm 25 \pm 17$
23-39%	$184 \pm 21 \pm 16$	$240 \pm 38 \pm 39$
39-77%	$166 \pm 20 \pm 14$	$196 \pm 28 \pm 28$

TABLE III: Rapidity density, dN/dy , for ϕ 's in two rapidity bins, by centrality. Errors are statistical followed by systematic.

Centrality	$1.2 < y < 1.4$	$1.4 < y < 1.6$
0-5%	$0.252 \pm 0.083 \pm 0.040$	$0.385 \pm 0.086 \pm 0.050$
5-12%	$0.215 \pm 0.036 \pm 0.020$	$0.229 \pm 0.078 \pm 0.034$
12-23%	$0.120 \pm 0.045 \pm 0.026$	$0.199 \pm 0.063 \pm 0.052$
23-39%	$0.060 \pm 0.017 \pm 0.012$	$0.069 \pm 0.020 \pm 0.023$
39-77%	$0.015 \pm 0.005 \pm 0.004$	$0.017 \pm 0.005 \pm 0.005$

of the other hadrons and explore their dependence on centrality and beam energy.

A. Transverse-mass spectrum of the ϕ ; comparison to other species

In the most central bin ($\sigma/\sigma_{\text{geom}} = 0-5\%$), the inverse slope parameter is determined to be 234 ± 31 MeV around midrapidity. As motivated by hydrodynamic models [38], the inverse slope parameters for different particle species are expected to scale with species mass for particles that participate in the collective transverse flow. It is interesting to see whether the inverse slope for ϕ mesons fits into the systematic trend observed for the other hadrons. However, two known effects complicate the interpreta-

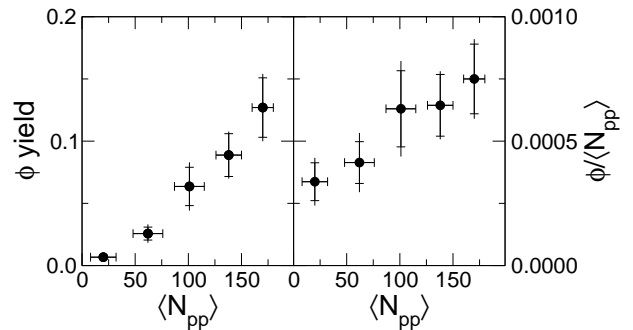


FIG. 6: The fiducial ϕ yield and fiducial yield of ϕ mesons per projectile participant, $\langle N_{\text{pp}} \rangle$, as a function of $\langle N_{\text{pp}} \rangle$. The accepted rapidity region is $1.2 < y < 1.6$. The error bars have the same significance as in Fig. 4.

tion.

The first is that the total cross section for the interaction of the ϕ with nucleons is about 8–12 mb [39], which is smaller than those for π 's, K 's and p 's by factors of 2–5 at AGS energies. The total $\phi\pi$ cross section is similarly speculated to be small, on the order of 1 mb [3]. ϕ 's might therefore be expected to decouple rather early from the nuclear fireball, which is composed of nucleon resonances and pions. Thus the ϕ inverse slope (T) will reflect the original “temperature” when the ϕ 's are produced, without the enhancement from collective transverse flow developed in the late hadronic stages [40]. In this case, T for the ϕ 's would be lower than that observed for other hadrons of similar mass (for example, p 's).

On the other hand, when the ϕ is detected via its decay into kaons, the rescattering of the daughter kaons from ϕ 's which decay inside the nuclear fireball would generate a relative depletion in the ϕ yield at low p_t . Given the short lifetime of the ϕ ($c\tau = 45$ fm/c), this effect would give rise to a strong depletion in the m_t spectrum only out to $m_t - m_0 = 0.1$ –0.2 GeV/c², *i.e.* only at the edge of the E917 acceptance. However, this effect could conceivably increase the apparent value of T in our fits to the m_t spectra. A similar explanation has been proposed [41] for the difference in the values of T for ϕ mesons obtained by experiments NA49 and NA50 which observed the ϕ via its decay into K^+K^- and $\mu^+\mu^-$ final states, respectively.

For the comparison of the transverse-mass spectra for various particle species, we choose to use the mean transverse mass, $\langle m_t \rangle$, rather than the inverse slopes themselves. The reason is that in Au + Au collisions at 11.7 GeV/c per nucleon, the spectra of some species, *e.g.* protons, is better described using a Boltzmann function,

$$\frac{1}{2\pi c^4 m_t} \frac{d^2 N}{dm_t dy} = \frac{dN/dy}{2\pi(T_B m_0^2 c^4 + 2T_B^2 m_0 c^2 + T_B^2)} \times m_t c^2 \exp\left(-\frac{(m_t - m_0)c^2}{T_B}\right), \quad (7)$$

than a simple exponential.

For this reason, only values of T_B (and not T) for protons have been reported [30, 42]. The values of $\langle m_t \rangle$ of all particle species in this study are either directly available in the references, or derived from the inverse-slope parameters, obtained with exponential (T) or Boltzmann (T_B) fits, as follows:

$$\langle m_t \rangle_{exp} = \frac{m^2 c^4 + 2mc^2 T + 2T^2}{mc^2 + T}, \quad (8)$$

$$\langle m_t \rangle_{Boltz} = \frac{m^3 c^6 + 3m^2 c^4 T_B + 6mc^2 T_B^2 + 6T_B^3}{m^2 c^4 + 2mc^2 T_B + 2T_B^2}. \quad (9)$$

The values of $\langle m_t - m_0 \rangle$ for ϕ mesons, together with the corresponding values for π 's, K 's, p 's, d 's, and $\bar{\Lambda}$'s produced at midrapidity in central Au + Au collisions at AGS energies [9, 12, 30, 42, 43] are plotted as a function of species mass in Fig. 7. We note that the centrality

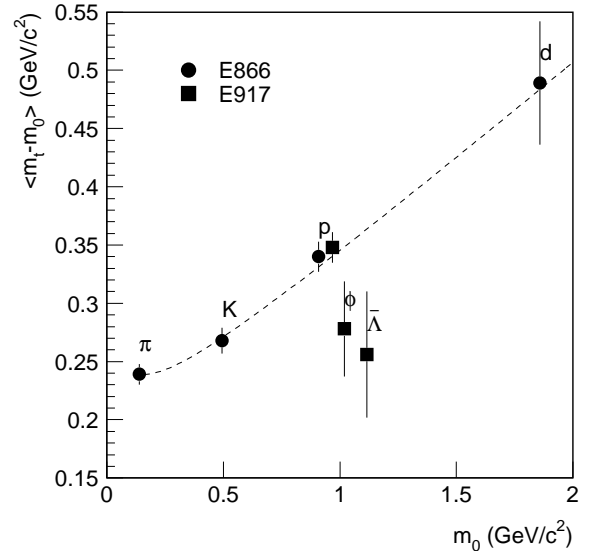


FIG. 7: The mean transverse mass ($\langle m_t - m_0 \rangle$) for various particle species as a function of the species mass at midrapidity for central Au+Au collisions at 11.7 GeV/c per nucleon as measured by E866 and E917. The dashed line is a fit assuming exponential transverse spectra and a linear relationship between inverse slope (T) and particle mass (m_0), as described in the text. Values for particles other than the ϕ are taken from Refs. [9, 12, 30, 42]. The proton data from E866 (E917) is presented with a shift of -30 MeV/c² ($+30$ MeV/c²) in mass for clarity.

selection differs somewhat from species to species in the available data: top 3% for π , p (E866), and d ; top 5% for p (E917), ϕ and K ; and top 12% for $\bar{\Lambda}$. Assuming exponential transverse spectra (Eq. (8)) and a linear relationship between inverse slope (T) and particle mass (m_0), $T = a + bm_0 c^2$ with a and b free parameters, a fit to the values of $\langle m_t - m_0 \rangle$ for π 's, K 's, p 's and d 's is shown as the dashed line.

The $\langle m_t - m_0 \rangle$ of the ϕ 's, together with the $\bar{\Lambda}$, fall below the trend of π 's, K 's, p 's, and d 's; this may indicate a systematic trend consistent with the early freeze-out of strange hadrons with small hadronic cross sections and a late development of at least some of the transverse flow, as suggested in Ref. [40].

B. Centrality dependence of ϕ production; comparison to other species

As mentioned in the Sec. I, processes such as $pp \rightarrow pp\phi$ are suppressed by large threshold energies and the OZI effect. Thus a naive expectation assuming ordinary hadronic interactions is that if an enhancement in ϕ production were observed in heavy-ion collisions at AGS energies, then this enhancement would result from sec-

ondary collisions, *e.g.* via channels such as $K^+\Lambda \rightarrow \phi p$ or $K^+K^- \rightarrow \phi\rho$ [24]. If this were in fact the case, increasing KY and KK combinatorics would bring about an increase of the ϕ/K ratio for central collisions.

On the other hand, the proposed “re-arrangement” [20] or “shake-out” [21] of an intrinsic $s\bar{s}$ component of the nucleon wave function in the non-perturbative regime provides a mechanism for ϕ production in $N+N$ interactions, which bypasses the effects of OZI suppression. Entrance-channel effects in reactions such as $p+p \rightarrow pp\phi$ may make this mechanism particularly important at energies near threshold (see Ref. [44] and references therein). Indeed, the DISTO collaboration has observed that in $p+p$ collisions at $\sqrt{s} = 2.90$ GeV, only 83 MeV above threshold, the ϕ/K^- ratio is about unity, such that ϕ production represents an important contribution to the K^- yield at these energies.

Along these lines, a possible mechanism has been proposed to explain overall strangeness production in $N+A$ collisions within the framework of the additive quark model [45]. According to this proposal, strange particles are born as strange-quark pairs from binary collisions of the projectile and target nucleons, with a probability proportional to the number of interacting constituent projectile quarks [46]. In $p+Au$ collisions at 17.5 GeV/ c , E910 has shown that the production of Λ ’s and K_S ’s increases with the estimated number of binary collisions, ν , suffered by the incident proton [19]. For $\nu \leq 3$, the increase of yields is faster than expected from scaling of $p+p$ data by the number of total participants (*i.e.*, $N^{p+A}/N^{p+p} = \frac{1}{2}(1+\nu)$), although bounded from above by linear scaling with ν (*i.e.*, $N^{p+A}/N^{p+p} = \nu$).

If the same mechanism were responsible for the observed increase in ϕ production with centrality in $A+A$ collisions, we would expect to observe similar scaling behavior in our data. Specifically, we would expect approximately constant numbers of hadrons bearing strange quarks to be produced per binary collision. In the following, we therefore compare the yield of ϕ ’s to the yields of pions and kaons as a function of centrality. The yields of pions and kaons were obtained by the E866 collaboration from $Au+Au$ collisions at the same beam energy used for the present measurement [9, 42].

As seen from the left panel of Fig. 8, the ϕ/π ratio of fiducial yields shows a rise toward central collisions, which signals an enhancement in the production of ϕ mesons relative to that of non-strange π mesons in central collisions. This enhancement is also clearly suggested by Fig. 6, since pion production is known to mainly come from resonance decay and secondary rescattering and scales linearly with $\langle N_{pp} \rangle$. Due to the fact that the plotted points represent ratios of fiducial yields, some care should be taken when interpreting the exact form of the dependence. We note that this increase in the ϕ/π ratio is qualitatively similar to the increase in the K/π ratio with centrality observed by E866 in $Au+Au$ collisions at the AGS [42].

We next compare the degree of enhancement in the

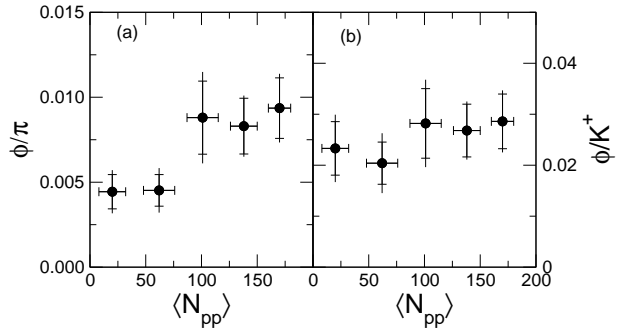


FIG. 8: The ϕ/π and ϕ/K^+ ratios as a function of $\langle N_{pp} \rangle$. For the ϕ , the fiducial yields from E917 in the rapidity interval $1.2 < y < 1.6$ are used. For π ’s, the data have been taken from Ref. [42], and represent fiducial yields in the rapidity interval $1.2 < y < 1.4$. The value used for the π yield is 1.125 times the yield for π^+ , which is essentially the average yield for π^+ and π^- [43]. For K^+ ’s, the data have been taken from Ref. [9], and represent fiducial yields in the rapidity interval $1.2 < y < 1.6$.

yields of ϕ ’s and K ’s, which both contain s quarks. We use the yield of K^+ to characterize the overall kaon production because the E866 data indicate that the K^-/K^+ ratio is about 0.15 and independent of centrality. In the right plot of Fig. 8, the ratio of fiducial yields ϕ/K^+ is plotted as a function of centrality, and shows no substantial variation. This implies that both ϕ and K^+ (or K^-) possess a similar degree of enhanced production toward central collisions at AGS energies. Estimated by linear fits to the ϕ/K^+ ratios as a function of $\langle N_{pp} \rangle$, an increase of up to 50% for the ratio in the most central bin cannot be definitively ruled out within 1σ range of the fitted errors. However, any centrality dependence of the ϕ/K ratios appears to be weak.

To look for scaling behavior similar to that observed in $p+Au$ collisions by E910, we examine the dependence of the ϕ yields in our data on the mean number of binary collisions, $\langle N_{coll} \rangle$. (Estimation of $\langle N_{coll} \rangle$ is discussed in Sec. II; the values of $\langle N_{coll} \rangle$ for each centrality bin are given in Table I.) The fiducial ϕ yield normalized to $\langle N_{coll} \rangle$ is plotted versus $\langle N_{coll} \rangle$ in Fig. 9. We observe that the fiducial ϕ yield is consistent with scaling proportional to $\langle N_{coll} \rangle$.

While the rapidity coverage of our measurement does not allow us to make a precise statement about the absolute value of the ϕ yield, it is possible to make an informed guess about the width of the ϕ rapidity distribution. Both E859 [4] and NA49 [5, 47] have observed that the Gaussian width of the ϕ rapidity distribution is very similar to those of the K^+ and K^- rapidity distributions. In central $Au+Au$ collisions at the AGS, the Gaussian widths of the rapidity distributions for K^+ and K^- are ~ 0.9 and ~ 0.7 , respectively [9, 25]. The narrow K^- width has been attributed to the higher threshold and more restricted phase space for K^- production. Since the thresholds for K^- and ϕ production in $p+p$ col-

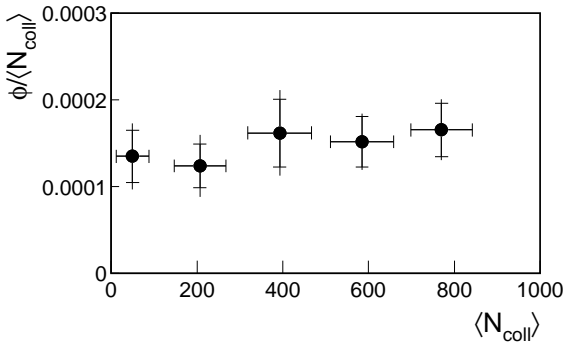


FIG. 9: The normalized fiducial yield of ϕ mesons per number of binary collisions, $\langle N_{\text{coll}} \rangle$, as a function of $\langle N_{\text{coll}} \rangle$. The accepted rapidity region is $1.2 < y < 1.6$.

lisions are very similar, we assume that the ϕ and K^- have Gaussian rapidity distributions with approximately equal widths in central Au + Au collisions. We then estimate that our fiducial yield corresponds to about 20% of the total yield. Using the parameterization described in Appendix A for the ϕ yield in $p + p$ collisions as a function of center of mass energy, \sqrt{s} , the yield of ϕ 's per binary collision in Au + Au collisions is about 50% of the ϕ yield in $p + p$ collisions at this energy. This observation seems contrary to the usual expectation of enhanced strangeness production in Au + Au collisions. We discuss this point further in Sec. IV C.

Using E866 data of the total yield of K^+ and K^- normalized to $\langle N_{\text{coll}} \rangle$, a similar scaling proportional to $\langle N_{\text{coll}} \rangle$ in the centrality is observed. It appears as if the mechanisms for the production of K^+ 's, K^- 's, and ϕ 's all have a similar dependence on the centrality of the collisions, and this dependence is consistent with a scaling with the number of binary collisions, $\langle N_{\text{coll}} \rangle$. This observation suggests that the hard binary collisions might play an important role in the strangeness production in heavy ion collisions.

Our observation that ϕ and kaon production scale similarly and faster than linearly with $\langle N_{\text{pp}} \rangle$ therefore provides an essential test of the details contained within rescattering models. The rescattering model, which suggested the importance of contributions from KY and KK collisions in the increase of ϕ production in the central A + A collisions [24], can be ruled out; if such contributions were dominant, combinatorial considerations would lead to the expectation that ϕ production should increase faster than kaon production with centrality. This is contradictory with our observation that ϕ and kaon production show similar scaling with centrality.

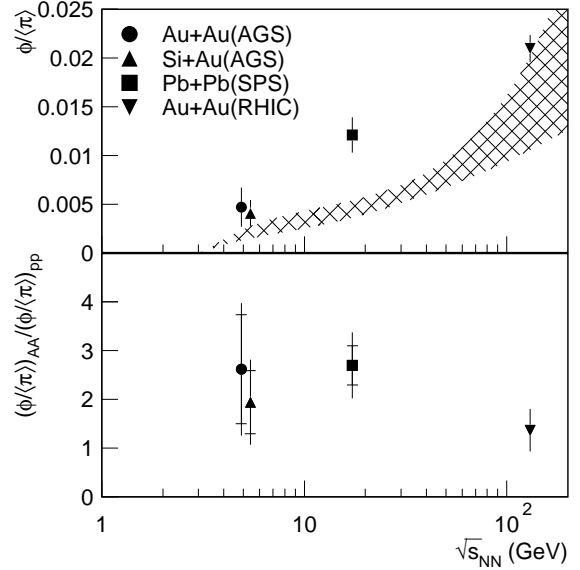


FIG. 10: Ratios of $\phi/\langle \pi \rangle$ in central heavy-ion and $p + p$ interactions as a function of $\sqrt{s_{\text{NN}}}$ (top panel) and double ratios of A + A over $p + p$ (bottom panel). For the E917 and STAR points, fiducial yield ratios are plotted; for the other two points, total yield ratios are shown instead. The hatched area represents the ratio of total yields in $p + p$ collisions, based on the parameterization discussed in the Appendix A. The cross bars in the bottom panel indicate the uncertainty range from the error of $\phi/\langle \pi \rangle$ in central heavy-ion interactions only.

C. Dependence of ϕ/π , ϕ/K^+ , and ϕ/K^- ratios on $\sqrt{s_{\text{NN}}}$ in A + A and $p + p$ reactions

In order to further explore the mechanism responsible for the approximate scaling of the ϕ yield with $\langle N_{\text{coll}} \rangle$ observed in our data, we compare our results with other measurements of ϕ production in heavy-ion collisions at different reaction energies.

The excitation functions of the ϕ/π , ϕ/K^+ , and ϕ/K^- ratios in central heavy-ion collisions are shown in Figs. 10, 11, and 12. The four points correspond to Au + Au collisions at the AGS (this measurement, $\sqrt{s_{\text{NN}}} = 4.87$ GeV) [9, 42], Si + Au collisions at the AGS ($\sqrt{s_{\text{NN}}} = 5.39$ GeV) [4, 8, 25], Pb + Pb collisions at the SPS ($\sqrt{s_{\text{NN}}} = 17.27$ GeV) [5, 47], and Au + Au collisions at RHIC ($\sqrt{s_{\text{NN}}} = 130$ GeV) [7, 14]. These plots must be interpreted with some care. Most obviously, the collisional system is different in each case; in particular, the various particle yields are not guaranteed to scale in the same way when passing from the Si + Au system to the heavier systems. In addition, the points for Au + Au collisions at the AGS and RHIC represent fiducial-yield ratios (the AGS point is for the fiducial yield over $1.2 < y < 1.6$, and the RHIC point is for the central unit of rapidity), while the other two points are ratios of yields over all

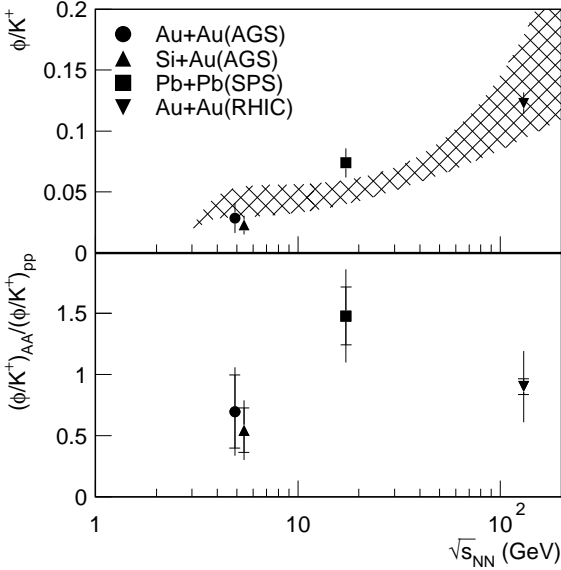


FIG. 11: Same as Fig. 10 for the ratios of ϕ/K^+ .

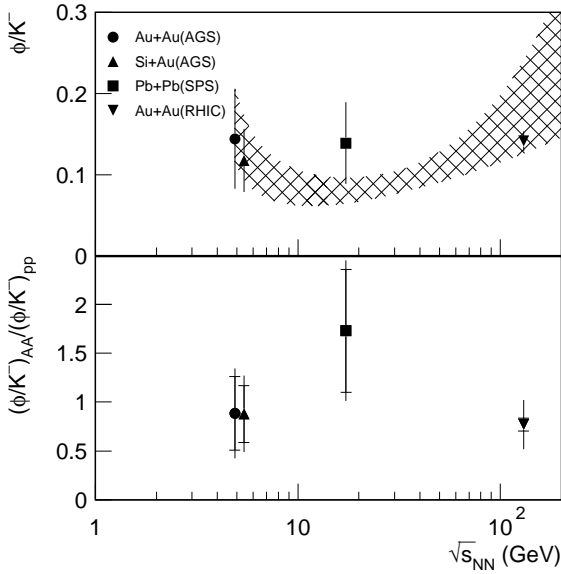


FIG. 12: Same as Fig. 10 for the ratios of ϕ/K^- .

phase space. Nor have we applied any corrections in the comparisons with $p+p$ collisions, taking into account the isospin averaging of yields from $p+p$, $n+n$, and $p+n$ collisions [9, 25, 48]. Nevertheless, two observations can be made.

Our first observation is that the ϕ/π ratios for $A+A$ collisions are notably enhanced with respect to their values for $p+p$ collisions for all points except at the highest

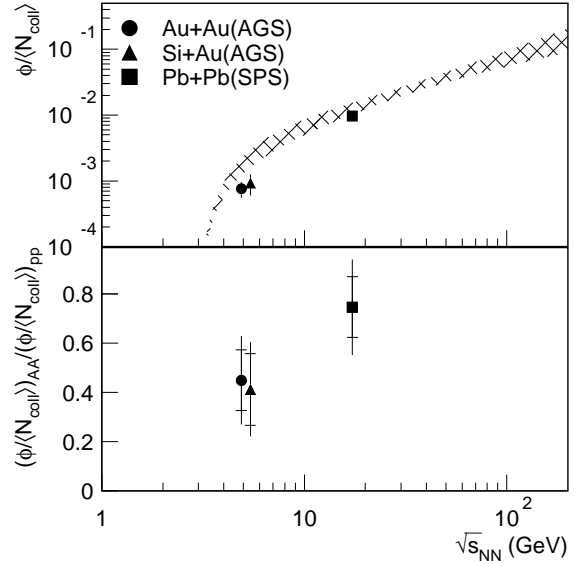


FIG. 13: Same as Fig. 10 for the ratios of $\phi/\langle N_{\text{coll}} \rangle$, where $\langle N_{\text{coll}} \rangle$ is the number of binary collisions. For E917 data point, an estimated total ϕ yield is plotted as described in the text.

energy in Fig. 10. In $p+p$ collisions, ϕ/π increases with $\sqrt{s_{NN}}$, in large part because of the larger production threshold for ϕ mesons. In heavy-ion collisions, the ϕ/π ratios are enhanced by factors of 2–3, at least up to SPS energies, but seem to show the same energy dependence observed in $p+p$ collisions, at least up to SPS energies. Such an enhancement in the central $A+A$ collisions could be interpreted by the different scaling behaviors of ϕ and π with centrality. As we discussed in Sec. IV B, the yield of ϕ 's scales with $\langle N_{\text{coll}} \rangle$ while that of π 's scales with $\langle N_{pp} \rangle$. The ratio of $\langle N_{\text{coll}} \rangle$ to $\langle N_{pp} \rangle$ is around 1 in the peripheral collisions, close to $p+p$ collisions, and becomes larger than 1 in the central collisions. At RHIC, the ϕ/π for central $Au + Au$ collisions is about the same as that from a parameterization of the $p+p$ data. It might be speculated that the primary production channels for ϕ 's or (and) π 's at RHIC energies are different from those at AGS and SPS energies.

The second observation is that the ϕ/K ratios for $A+A$ collisions are only marginally enhanced with respect to their values for $p+p$ collisions, and show relatively little variation as a function of energy as seen in Fig. 11 and Fig. 12. Our parameterization of the $p+p$ cross section for ϕ production suggests that the ϕ/K^- ratio increases as $\sqrt{s_{NN}}$ approaches the threshold value from above for the reaction $pp \rightarrow pp\phi$. The ϕ/K^- ratios in heavy-ion data seem to follow the energy dependence observed in $p+p$ collisions rather reasonably.

It is interesting to see if the data points from other systems and energies obey the scaling with $\langle N_{\text{coll}} \rangle$ as well. The ratio $\phi/\langle N_{\text{coll}} \rangle$ for central $A+A$ collisions at the

AGS and SPS is plotted in Fig. 13. For the comparison, we are forced to assume a value for the ϕ rapidity width for our measurement. A width of $\sigma_y = 0.71$ equal to the measured K^- width is used, as explained in the previous section, and we plot our point with an additional 20% systematic uncertainty corresponding to a range of values for σ_y from 0.6 (overlap of K^+ and K^- rapidity distributions) to 0.9 (K^+ rapidity distribution). The RHIC point is not included in this comparison, because there is no reasonable way to extrapolate the fiducial yield to all of phase space. The ratio $(\phi/\langle N_{\text{coll}} \rangle)_{\text{A}+\text{A}} / (\phi/\langle N_{\text{coll}} \rangle)_{p+p}$ is consistent with $\sim 0.5\text{--}0.7$ for all three points from the AGS and SPS. Our comparison is by no means precise. However, it does seem that the yield of ϕ 's per binary collision, modulo the effects of threshold and center-of-mass energy dependence, is approximately constant across the three collisional systems studied. Furthermore, instead of an enhancement of ϕ yields per binary collisions in heavy-ion collisions, this double ratio is less than 1. This might reflect the effect of ϕ absorption in the nuclear fireball after being produced, as the inelastic cross section of ϕ with nucleons ($\cong 8\text{--}10$ mb [49]) is a significant component of the total interaction cross section ($\cong 8\text{--}12$ mb).

V. SUMMARY

In conclusion, we have studied ϕ production in Au+Au collisions at $11.7A\text{ GeV}/c$ around midrapidity as a function of collision centrality. The yield per projectile participant shows a steady rise toward central collisions. This enhanced production in central collisions is stronger than that of non-strange π mesons as seen from the increasing ϕ/π ratio with centrality. The ratios ϕ/K^+ and ϕ/K^- are approximately constant with $\langle N_{\text{pp}} \rangle$. The yield of ϕ 's, like the yields of K^+ and K^- , is seen to scale with $\langle N_{\text{coll}} \rangle$, the number of binary collisions, and this observation is against the prediction from the rescattering models of ϕ production. Finally the yield of ϕ 's per binary collision in A+A collisions is about 50–70% of the ϕ yield in $p+p$ collisions at AGS and SPS energies. That the yield of ϕ 's per binary collision in A+A collisions is smaller than that in $p+p$ collisions might signal the effect of ϕ absorption by nucleons in the heavy-ion collisions.

Acknowledgments

This work has been supported by the U.S. Department of Energy under contracts with ANL (No. W-31-109-ENG-38), BNL (No. DE-AC02-98CH10886), MIT (No. DE-AC02-76ER03069), UC Riverside (No. DE-FG03-86ER40271), UIC (No. DE-FG02-94ER40865), and the University of Maryland (No. DE-FG02-93ER40802); by the National Science Foundation under contract with the University of Rochester (No. PHY-9722606); and by the Ministry of Education and KOSEF (No. 951-0202-032-2) in Korea.

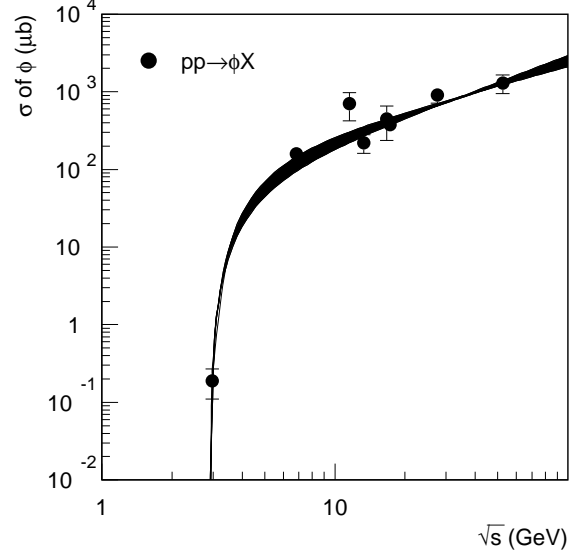


FIG. 14: Parameterization of the ϕ yield in $p+p$ interactions. The data points are from Refs. [5, 44, 50]. The fit is discussed in the text.

APPENDIX A: PARAMETERIZATION OF ϕ PRODUCTION AS A FUNCTION OF \sqrt{s} IN $p+p$ COLLISIONS

The ϕ yield in $p+p$ collisions provides a useful benchmark for the interpretation of ϕ yields in heavy-ion collisions. There are various existing measurements of the inclusive total cross section for ϕ production in $p+p$ collisions for $5 < \sqrt{s} < 60$ GeV [5, 44, 50] that can be extrapolated to the values of $\sqrt{s_{NN}}$ for which heavy-ion data exist. (Note that the point at $\sqrt{s} = 2.90$ GeV from Ref. [44], while technically an exclusive measurement in the $pp \rightarrow ppK^+K^-$ channel, is also an inclusive measurement, since no other channels with a ϕ or K^- in the final state are kinematically allowed at this energy.) We have fitted these measurements with a form used to parameterize results on vector meson production cross sections in $p+p$ collisions obtained from one-pion exchange calculations [51] and the Lund String Model [52]:

$$\begin{aligned} \sigma(pp \rightarrow \phi X) &= a(1-x)^b x^c \\ x &\equiv s_{\text{thresh}}/s \\ s_{\text{thresh}} &= 8.38 \text{ GeV}^2 \end{aligned} \quad (\text{A1})$$

The results of our fit are shown in Fig. 14. We obtain $a = 74^{+36}_{-24} \text{ mb}$, $b = 2.05^{+0.22}_{-0.18}$, and $c = 1.56^{+0.30}_{-0.27}$. For comparison with heavy-ion data, we obtain yields by dividing the ϕ cross sections for each value of $\sqrt{s_{NN}}$ by the inelastic $p+p$ cross section. For Au+Au collisions at the AGS, $\sqrt{s_{NN}} = 4.87$ GeV, and our parameterization

of the $p+p$ data gives a yield of 0.00169 ± 0.00042 at this energy.

For K and π production in $p+p$ reactions, we use the

multiplicity parameterizations in Ref. [53]. The smallest \sqrt{s} for the ranges of parameterization for π , K^+ and K^- are 3.0, 2.98 and 5.03 GeV, respectively.

[1] S. Okubo, Phys. Lett. B **5**, 165 (1963); G. Zweig, CERN report NO. 8419/TH, 412 (1964); I. Iizuka, Prog. Theor. Phys. Suppl. **37/38**, 21 (1966).

[2] P. Koch, B. Müller, and J. Rafelski, Z. Phys. A **324**, 453 (1986).

[3] A. Shor *et al.*, Phys. Rev. Lett. **54**, 1122 (1985).

[4] Y. Akiba *et al.*, Phys. Rev. Lett. **76**, 2021 (1996).

[5] S.V. Afanasiev *et al.*, Phys. Lett. B **491**, 59 (2000).

[6] M.C. Abreu *et al.*, J. Phys. G **27**, 405 (2001); M.C. Abreu *et al.*, Nucl. Phys. A **661**, 534c (1999).

[7] C. Adler *et al.*, Phys. Rev. C **65**, 041901(R) (2002).

[8] T. Abbott *et al.*, Phys. Rev. Lett. **64**, 847 (1990).

[9] L. Ahle *et al.*, Phys. Rev. C **58**, 3523 (1998).

[10] L. Ahle *et al.*, Phys. Lett. B **476**, 1 (2000).

[11] T.A. Armstrong *et al.*, Phys. Rev. C **59**, 2699 (1999).

[12] B.B. Back *et al.*, Phys. Rev. Lett. **87**, 242301 (2001).

[13] E. Anderson *et al.*, Phys. Lett. B **433**, 209 (1998); E. Anderson *et al.*, Phys. Lett. B **449**, 401 (1999).

[14] K. Adcox *et al.*, Phys. Rev. Lett. **88**, 192302 (2002).

[15] R. Mattiello *et al.*, Phys. Rev. Lett. **63**, 1459 (1989).

[16] Y. Pang, T.J. Schlagel, and S.H. Kahana, Phys. Rev. Lett. **68**, 2743 (1992).

[17] B.A. Li and C.M. Ko, Phys. Rev. C **52**, 2037 (1995).

[18] P. Braun-Munzinger *et al.*, Phys. Lett. B **344**, 43 (1995); J. Cleymans *et al.*, Z. Phys. C **74**, 319 (1997).

[19] I. Chemakin *et al.*, Phys. Rev. Lett. **85**, 4868 (2000).

[20] M.B. Green *et al.*, Nuovo Cimento A **29**, 123 (1975); A. Donnachie, P.V. Landshoff, Nucl. Phys. B **112**, 233 (1976).

[21] J. Ellis *et al.*, Phys. Lett. B **353**, 319 (1995).

[22] W.S. Chung *et al.*, Phys. Lett. B **401**, 1 (1997).

[23] M. Berenguer *et al.*, Phys. Lett. B **332**, 15 (1994).

[24] C.M. Ko and B.H. Sa, Phys. Lett. B **258**, 6 (1991).

[25] L. Ahle *et al.*, Phys. Rev. C **60**, 044904 (1999).

[26] F.Q. Wang, J. Phys. G : Nucl. Part. Phys. **27**, 283 (2001).

[27] J.C. Dunlop and C.A. Ogilvie, Phys. Rev. C **61**, 031901 (2000).

[28] L. Ahle *et al.*, Phys. Lett. B **490**, 53 (2000).

[29] B.B. Back *et al.*, Phys. Rev. Lett. **86**, 1970 (2001).

[30] B.B. Back *et al.*, Phys. Rev. C **66**, 054901 (2002).

[31] T. Abbott *et al.*, Nucl. Instrum. Meth. A **290**, 41 (1990).

[32] H. Xiang, Ph.D. Thesis, Univ. of California, Riverside, 1999; J.C. Dunlop, Ph.D. Thesis, MIT, 1999; G. Heintzelman, Ph.D. Thesis, MIT, 1999; M.D. Moulson, Ph.D. Thesis, Columbia Univ., 2001.

[33] W.A. Zajc, “The E859 level II trigger system”, AIP Conference Proceedings, Volume **243**, Issue 1, 415 (1992).

[34] R.J. Glauber and G. Matthiae, Nucl. Phys. B **21**, 135 (1970).

[35] T. Abbott *et al.*, Phys. Rev. C **44**, 1611 (1991).

[36] G.I. Kopylov, Phys. Lett. B **50**, 472 (1974).

[37] J.D. Jackson, Nuovo Cimento **34**, 6692 (1964).

[38] E. Schnedermann, J. Sollfrank, and U. Heinz, Phys. Rev. C **48**, 2462 (1993).

[39] G. McClellan *et al.*, Phys. Rev. Lett. **26**, 1593 (1971); H.-J. Behrend *et al.*, Phys. Lett. B **56**, 408 (1975); T.H. Bauer *et al.*, Rev. Mod. Phys. **50**, 261 (1978);

[40] H. van Hecke, H. Sorge, and N. Xu, Phys. Rev. Lett. **81**, 5764 (1998).

[41] E.V. Shuryak, Nucl. Phys. A **661**, 119c (1999).

[42] L. Ahle *et al.*, Phys. Rev. C **59**, 2173 (1999).

[43] L. Ahle *et al.*, Phys. Rev. C **57**, R466 (1998).

[44] F. Balestra *et al.*, Phys. Rev. C **63**, 024004 (2001).

[45] V.V. Anisovich *et al.*, Nucl. Phys. B **133**, 477 (1978).

[46] K. Kadija *et al.*, Z. Phys. C **66**, 393 (1995).

[47] S.V. Afanasiev *et al.*, Phys. Rev. C **66**, 054902 (2002).

[48] M. Gazdzicki and O. Hansen, Nucl. Phys. A **528**, 754 (1991).

[49] R. Bailey *et al.*, Z. Phys. C **22**, 125 (1984).

[50] F. Balestra *et al.*, Phys. Lett. B **468**, 7 (1999); V. Blobel *et al.*, Phys. Lett. B **59**, 88 (1975); M. Antipov *et al.*, Phys. Lett. B **110**, 326 (1982); C. Daum *et al.*, Nucl. Phys. B **186**, 205 (1981); D. Drijard *et al.*, Z. Phys. C **9**, 293 (1981).

[51] A.A. Sibirtsev, Nucl. Phys. A **604**, 455 (1996).

[52] W. Cassing and E.L. Bratkovskaya, Phys. Rept. **308**, 65 (1999).

[53] A.M. Rossi *et al.*, Nucl. Phys. B **84**, 269 (1975).